Anisotropic Charge Transport and Spin−Spin Interactions in K^+(Cryptand [2.2.2]) Electride

Andrew S. Ichimura,† Michael J. Wagner,‡ and James L. Dye*

Department of Chemistry, Michigan State University, East Lansing, Michigan 48823-1322

Received: July 1, 2002

Single-crystal conductivity measurements of the electride K^+(cryptand[2.2.2])e^- show pronounced anisotropy. Conductivity of the sheetlike crystals is 10−30 times greater in the "easy" than in the "hard" in-plane direction and 10^5−10^6 times greater than that perpendicular to the plane. The magnetic susceptibility is well-described by the alternating linear chain Heisenberg antiferromagnetic model. Both phenomena are consistent with the structure, which has very open pseudo-1D channels that connect large dumbbell-shaped two-electron cavities to form a chain of coupled electron spins. Slightly smaller channels interconnect these chains to form a 2D network of channels and cavities. The proposed conductivity mechanism is the random 2D hopping of hole defects that are highly mobile down the open 1D chain. They undergo activated transport to adjacent chains as a result of defect sites (such as K^-) in the primary chain.

Introduction

The electride, K^+(cryptand[2.2.2])e^- (abbreviated K^+C222e^-), has a much greater electrical conductivity and much stronger antiferromagnetic coupling than any other electride of known structure.[1−3] The cavity−channel geometry[4] suggests that the properties would be strongly anisotropic, with essentially 1D spin−spin coupling. Thin-film optical and conductivity studies[5] suggested that defects such as missing electrons (holes) are the primary charge carriers. It was proposed that 1D defect motion down the main channels is very facile and is accompanied by activated interchain hopping of electrons or holes at channel-blocking sites.[5] Powder conductivity studies indicated that grain-boundary resistance is also important.[2] In this paper, we show that the magnetic susceptibility is well described by the 1D alternating linear chain Heisenberg antiferromagnetic (ALCHA) model.[6,7] Four-probe single-crystal impedance measurements demonstrate that the conductivity is highly anisotropic and is primarily in the plane of the 2D channel system.

Seven crystalline electrides have now been synthesized and structurally characterized.[8,9] All have alkali cations encapsulated within cryptands or sandwiched between crown ether molecules. They are similar in structure to crystalline alkalides in which the cationic charge is balanced by alkali metal anions, Na^-, K^-, Rb^-, or Cs^-.[10] Both experiment and theory strongly indicate that the electron density is concentrated in the otherwise empty anionic sites—cavities of diameter 4.5−6.0 Å.[11,12] Thus, to first order, electrides can be viewed as stoichiometric F-centers in which essentially *all* anionic sites contain trapped electrons. If the centers were cut off from each other by sections of the organic complexant, then electrides could be viewed as a collection of electrons in "spherical boxes". Because electrons have a spin of $^1/_2$, the magnetic susceptibility of isolated electrons would obey the Curie law,

$$\chi = C/T \tag{1}$$

Curie law behavior is, in fact, seen in alkalide−electride mixtures in which only a small fraction of the cavities contain electrons and most contain diamagnetic alkali metal anions.

The crystal structures of electrides show, however, that the cavities are connected by channels.[4] The sizes of these channels vary from one electride to another. Five of the seven electrides of known structure have essentially 1D chains of cavities and channels, similar to beads on a string. Although other channels interconnect these chains, they are smaller, more tortuous, and longer than the primary channels. As a result, electrons in adjacent cavities are coupled antiferromagnetically. Intrachain coupling dominates the magnetic properties, and the behavior is well-described by the linear chain Heisenberg antiferromagnetic (LCHA) model.[13] The coupling constant J is negative, and its magnitude increases monotonically with an increase in the cross-sectional area of the major connecting channel.[8,9]

Even though each electron is magnetically coupled with two nearest neighbors, all of these electrides are insulators, defect conductors, or semiconductors.[2] The energy cost of placing two electrons in the same cavity is evidently too great to support electron mobility down the chain, so these electrides are Mott insulators.[14]

The title electride, K^+C222e^-, has a fundamentally different cavity−channel geometry than the five predominantly 1D electrides described above. (The seventh electride has a mixture of 15-crown-5 and 18-crown-6 molecules and a complex structure.[15,16]) The crystal structure of K^+C222e^- shows the presence of dumbbell-shaped cavities about 11 Å long. The maximum cavity diameter is 4.6 Å with a central "pinch" that is 4.2 Å in diameter. In the corresponding alkalides, K^+C222K^- and $Rb^+C222Rb^-$, each of these dumbbell cavities contains alkalide dimers, $(M_2)^{2-}$.[17] In K^+C222e^-, each of these two-electron cavities is connected chainwise to adjacent dumbbells by straight, wide channels of minimum diameter 3.6 Å. Secondary bent channels of minimum diameter 2.3 Å connect adjacent cavity−channel chains to form a 2D network. Channels that connect these 2D arrays into a 3D network are only 0.8 Å

* Corresponding author. E-mail: dye@msu.edu.
† Current address: Department of Chemistry, San Francisco State University, 1600 Holloway Avenue, San Francisco, California 94132.
‡ Current address: Department of Chemistry, The George Washington University, Corcoran Hall 725, 21st Street N.W., Washington, D.C. 20052.

10.1021/jp026420n CCC: $22.00
Published on Web 10/05/2002

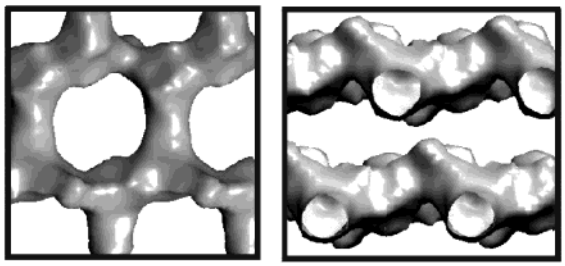

Figure 1. Two views of the channel structure of $K^+(C222)e^-$. The view on the left shows the collection of channels that form the pseudo-2D planes. The dumbbell-shaped cavities are nearly horizontal and are slanted upward from left to right, the open connecting channels are vertical, and the bent channels (nearly horizontal) are alternately up and down from the plane of the image as one moves from bottom to top. The view on the right is obtained by a 90° rotation of the left view about a horizontal axis.

in diameter. Figure 1, obtained from the crystal structure, shows the nature of these cavities and channels. In summary, the overall void space within this electride consists of an anisotropic mosaic of interconnected cavities and channels, with dominance by very open channels in one direction.

As is the case with four other electrides, $Rb^+(C222)e^-$ exists in two forms depending on the method of preparation and/or temperature. One of these forms, which we have designated form β,[9] has thin-film characteristics, conductivity, and magnetic susceptibility behavior that strongly suggest a structure similar to that of $K^+(C222)e^-$.

The experiments described in this paper support and refine prior hypotheses about the conduction mechanism, delineate the nature of defects in $K^+(C222)e^-$ and $Rb^+(C222)e^-$, and show that the cavity−channel structure makes these interpretations reasonable.

Experimental Section

Synthesis. The synthesis of $K^+(C222)e^-$ crystals and the purification of reagents was carried out according to established procedures.[9,10,13,18,19] In brief, a slight excess of purified cryptand[2.2.2] was placed on one side of a borosilicate K-cell, and potassium metal was distilled to form a mirror on the other side. Approximately 15 mL of dry, degassed dimethyl ether was distilled onto the complexant. The complexant was dissolved at or below −25 °C, and then the K-cell was cooled in a 2-propanol bath to −55 °C. The cryptand[2.2.2] solution was poured over the potassium mirror to form the dark-blue solution of the electride. To form a saturated solution suitable for crystal growth, 10 mL of diethyl ether was added, and some of the dimethyl ether was removed under vacuum until crystals of the electride began to appear on the surface of the liquid. A crop of crystals was grown by slowly cooling the reaction vessel from −55 to −75 °C over a 30 h period.

Magnetic Susceptibility. Crushed crystals of the electride were placed in a thin-wall 6-mm o.d. quartz tube and rested on a quartz septum. A small quantity of helium gas, ∼1 Torr, was introduced into the tube to facilitate heat transfer before the quartz was sealed off from the vacuum line. The tube was designed to have about 30 mm of quartz below the septum so that a more or less even response would be generated as the sample passed through the coils of the Quantum Design MPMS2 Squid magnetometer. The diamagnetic correction for the sample and holder was obtained by letting the electride decompose at elevated temperatures, and then the temperature program was rerun.

Impedance Spectroscopy. Crystals of $K^+(C222)e^-$ are black and platelike with a rhombic shape. Large crystals suitable for conductivity studies may be grown with dimensions that exceed 1 cm on a side but that are also paper-thin. A previous determination of the crystal structure[1,20] had shown that the crystal planes were parallel to the 2D array of interconnected cavities and channels. Because electrides readily decompose at temperatures above 230 K and in the presence of oxygen and moisture, all sample handling was carried out in a nitrogen-filled glovebag at temperatures near 77 K. The conductivity cells were precooled in a liquid nitrogen bath before the crystals were mounted. The impedance within the plane of the crystal was measured with a four-probe conductivity cell in which the spring-loaded electrodes were arranged in a square configuration with a 3-mm separation between contact points along one side of the square. A single crystal cut to dimensions 4 mm × 4 mm was placed in the bottom of a Delrin cup, and the spring-loaded electrodes were lowered onto the crystal. Because of handling difficulties, no attempt was made to correlate the placement of the electrodes with the crystal or cavity−channel structure except that the four probes were perpendicular to the crystal planes. To ensure good electrical contact, the tips of the spring-loaded gold electrodes were coated with a small quantity of potassium metal. This has the added benefit that electrode effects, such as the formation of a Schottky barrier at the probe−sample junction, are minimized.[2] In the impedance measurements, a constant voltage was applied between two of the electrodes, and the current and phase shift were measured across the other two electrodes. At each temperature, the electrodes were switched to measure the frequency dependence of the impedance in two perpendicular directions within the crystal plane.

The impedance perpendicular to the plane of the crystal was measured with a two-probe conductivity cell with one fixed and one movable electrode. In a helium-filled glovebox, potassium metal was applied to the electrode surfaces, and the electrodes were pressed together to form a uniform film of metal. After the cell was cooled in a liquid nitrogen bath, a single crystal of approximate dimensions 3 mm × 4 mm was placed directly onto the potassium film. The conductivity cell was assembled, and the electrodes were brought together until the resistance as measured with a Keithley electrometer dropped precipitously from the gigaohm to the 100-kΩ range, signifying that electrical contact had been made. In both the four- and two-probe impedance measurements, the frequency was stepped logarithmically between 5 Hz and 11.7 MHz at voltages between 40 mV and 1 V. A Hewlett-Packard 4192A low-frequency impedance analyzer interfaced to a Lab View program was utilized in this work.

EPR Spectra. EPR spectra were recorded with a Bruker ESP300E spectrometer and the following instrument settings: modulation amplitude 0.01 G, modulation frequency 1.5 kHz, 0.01 mW, sweep width and time of 50 G and 84 s, respectively. The temperature was controlled with an Oxford Instruments 900E liquid helium cryostat and a Bruker VT2000 nitrogen gas flow cryostat. In a nitrogen-filled glovebag, crystals of the electride were crushed in a mortar and pestle that had been precooled to liquid nitrogen temperature. About 1 mg of the resulting black powder was quickly transferred to a 4-mm o.d. quartz EPR tube, which was then sealed under vacuum at $\sim 10^{-5}$ Torr. EPR intensities were obtained by double integration of the signals.

Optical Spectra. Single crystals of freshly prepared $K^+(C222)e^-$ were transferred into a quartz optical cell (1-mm

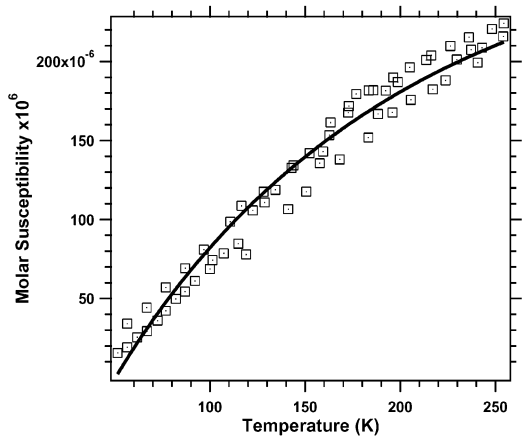

Figure 2. Molar susceptibility of $K^+(C222)e^-$ in the high-temperature region. The Curie tail has been subtracted. The solid line is the best fit to the ALCHA model.

path length) that was attached directly to the synthesis vessel (K-cell). The optical cell was sealed off under vacuum at −78 °C, thus ensuring that the surface of the crystals would remain pristine. Reflectance spectra were recorded in the specular reflection mode[21] with a Guided Wave model 260 spectrophotometer.

Results and Conclusions

Magnetic Susceptibility. The general behavior of the magnetic susceptibility of powdered samples of $K^+(C222)e^-$ as a function of temperature was reported in the original paper.[1] A preparation-dependent "Curie tail" that corresponded to 0.3 to 5.0% of the total amount of compound was followed by a gradual increase in the susceptibility with temperature. Our initial interpretation of the increase[1] suggested either population of a triplet state or dissociation of electron pairs. In the present work, additional susceptibility measurements were made on four separate samples of crushed crystals from two preparations. Because the rise with increasing temperature yields important information about interelectron coupling, the region from 50 to 250 K was studied in detail in one of the SQUID runs. Figure 2 shows the temperature dependence of the molar susceptibility in this region after subtraction of the Curie tail.

Thermal decomposition prevented studies above about 250 K, and the limited region and small signal made it difficult to determine the cause of the increasing susceptibility. Attempts to fit the data to the behavior expected for the thermal population of an accessible triplet state were unsuccessful. The excellent results obtained with other electrides by using the linear chain Heisenberg antiferromagnetic (LCHA) model[13] prompted us to try this model as well, but the fit was also very poor. The cavity−channel structure of this electride suggested that in addition to strong coupling to the nearest neighbor in the dumbbell-shaped cavity, next-nearest neighbor interactions through the very open, short channels would also be significant. We therefore applied the ALCHA model based on the Hamiltonian

$$H = -2J\sum_{i=1}^{n/2}[\hat{S}_{2i}\hat{S}_{2i-1} + \alpha\hat{S}_{2i}\hat{S}_{2i+1}] \qquad (2)$$

in which J is the exchange integral between a spin and its nearest neighbor and αJ is that for the next-nearest neighbor. There is no closed-form solution for the magnetic susceptibility based on this Hamiltonian, but a fit of numerical solutions to the model, on the basis of the work of Bonner and Fisher,[6,7] has been obtained. The molar susceptibility is given by

$$\chi = \frac{ng^2\beta^2}{kT}\left[\frac{A(\alpha) + B(\alpha)X + C(\alpha)X^2}{1 + D(\alpha)X + E(\alpha)X^2 + F(\alpha)X^3}\right] \qquad (3)$$

in which $X = |J|/kT$ and the terms $A-F$ are known functions of α.[22]

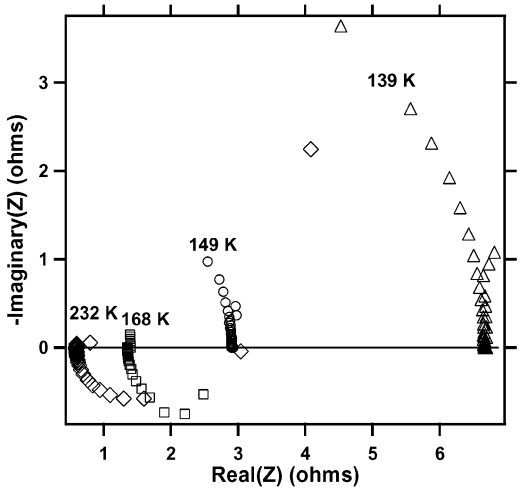

Figure 3. Impedance arcs at various temperatures along the in-plane easy direction with an applied voltage of 40 mV. The behavior at 1000 mV was nearly the same. The frequency was scanned logarithmically from 5 Hz to 13 MHz. At all temperatures, the real part of Z was essentially independent of frequency up to 1 MHz.

The solid line in Figure 2 shows that the agreement between this model and the data is satisfactory. The least-squares fit yields $-J/k = 440$ K, $\alpha = 0.86$. Whereas the standard deviation estimates are small for a given run, the value of $-J/k$ ranged from 300 K (for a sample that had the largest Curie tail) to 450 K, and α varied from 0.83 to 0.88 in three separate runs. The results shown in Figure 2 are for the most detailed study. They were obtained with freshly prepared crushed crystals that showed the lowest number of defect electrons (0.29%), as determined from the magnitude of the Curie tail. The parameters are essentially the same when data below 150 K are excluded.

The magnitude of the coupling constant for $K^+(C222)e^-$ is much greater than that of any other electride. The closest competitor is $Li^+(C211)e^-$, with $-J/k = 55$ K and an interelectron channel area that is only 60% as large.[23] As demonstrated in earlier papers,[8,9] a graph of $\ln(-J/k)$ versus the cross-sectional area of the channel between electron trapping sites yields a straight line for six electrides, including $K^+(C222)e^-$.

The contribution of the Curie tail increased upon partial decomposition, rising from 0.29 to 0.38 to 0.85% upon successively raising the temperature briefly above 240 and 250 K, respectively. Such an increase in the concentration of defects was proposed as the cause of the increased conductivity of thin films during the initial stages of decomposition.[5] Its significance will be considered in connection with the conductivity mechanism described later in this paper.

Impedance Spectra. The impedance spectra within and perpendicular to the crystal plane clearly show that the conductivity of $K^+(C222)e^-$ is highly anisotropic. Figures 3 and 4 show the impedance spectra measured within the plane of the crystal with the four-probe cell as a function of temperature. The DC resistance, R, obtained from the low-frequency intercept is approximately 10−30 times greater in one direction than in the other within the crystal plane at temperatures between 140

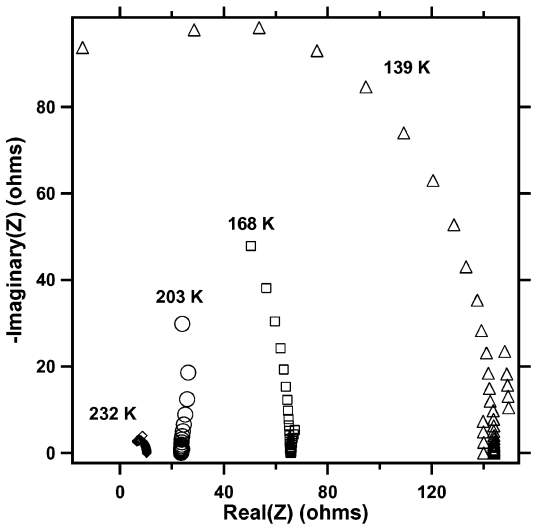

Figure 4. Impedance arcs at various temperatures along the in-plane hard direction with an applied voltage of 40 mV. The behavior at 1000 mV was nearly the same. At all temperatures, the real part of *Z* was essentially independent of frequency up to 0.5 MHz.

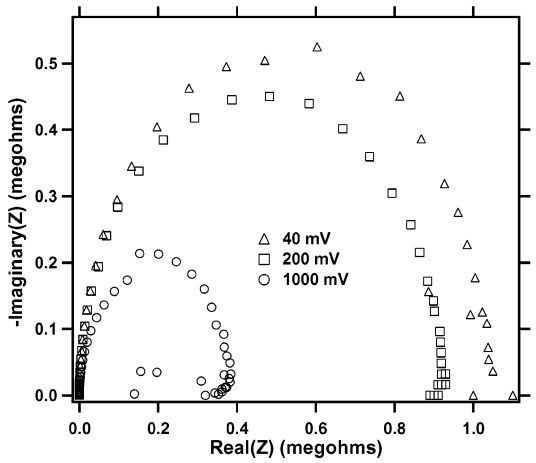

Figure 5. Impedance arcs in the direction perpendicular to the crystal plane at 246 K. Note the pronounced voltage dependence of the response. At lower temperatures, the impedance was beyond the range of the instrument. The five low readings at 1000 mV (○) were at frequencies below 50 Hz.

and 230 K. Because the orientation of the electrodes with respect to the crystallographic axes was unknown, the nomenclature "easy" and "hard" will refer to the directions within the crystal plane of the lesser and greater resistance, respectively. Thus, at 139 K, $R = 6.7\ \Omega$ ($\rho = 9.1\ \Omega$ cm) and 144 Ω ($\rho = 196\ \Omega$ cm) along the easy and hard directions, respectively. The electrical response of the system was linear in the applied voltage in both directions. This implies that good electrical contact was made between the electrodes and sample and that the system was free of blocking effects that might be caused by a potassium oxide layer on the electrode surface or from a Schottky barrier.

The response of the system to an alternating current is far from that of a typical RC circuit with a unique time constant. The real part of the impedance within the crystal plane was largely frequency-independent except at the highest frequencies and at the lowest temperatures. Typically, the imaginary part of the impedance decreased to near zero as the frequency was increased from 5 to ∼100 Hz and then remained relatively constant until frequencies greater than 1.0 MHz were applied. The corresponding phase shift of the measured current behaves similarly but was somewhat more sensitive to frequency. The result was that only partial impedance arcs were observed between 5 Hz and 11.7 MHz. In contrast to these in-plane single-crystal impedance spectra, previous measurements on pressed pellets of the electride typically showed nearly complete impedance arcs that were attributed to grain-boundary capacitances.[2] In the present measurements, the resistance was low enough that competing reactances and/or parasitics could account for much of the observed behavior as the temperature was raised. For example, as shown in Figure 3 for the easy direction, the impedance above 150 K lies in the fourth quadrant of the complex plane, suggesting that lead inductance becomes the dominant effect. The net result is only a small temperature dependence of the DC resistance, from 3.0 Ω at149 K to 0.7 Ω at 232 K. As shown in Figure 4, along the hard axis, the major response due to the AC signal as a function of temperature can be attributed to the sample resistance that varies from about 140 Ω at 139 K to ∼10 Ω at 232 K. The sample capacitance in both directions is apparently small; lead inductance and competing parasitic capacitances may account, at least in part, for the atypical impedance behavior.

As shown in Figure 5, the impedance arcs at 246 K perpendicular to the crystal plane are nearly complete and depend strongly on the applied voltage. The perpendicular direction has a resistance that is a factor of 10^5-10^6 greater than that within the crystal plane. The electrical response of the system is clearly nonlinear in this direction, despite the use of potassium-coated electrodes that typically lead to an ohmic response of the electrode−sample junction of pressed electride pellets, even in two-probe conductivity cells. The magnitude of the resistance was near the limit of our instrumentation, and only at the highest temperatures were clear impedance arcs observed. This behavior is consistent with a substantial barrier to charge mobility perpendicular to the crystal plane.

The cavity−channel model of $K^+(C222)e^-$ shown in Figure 1 provides an explanation for the anisotropic resistivity. The crystal structure shows that within the crystal plane, open short channels 3.6 Å in diameter and bent channels 2.3 Å in diameter connect the large dumbbell-shaped cavities at both ends to form a continuous 2D array. Narrow, longer channels only 0.8 Å in diameter intersect the minor 2.3-Å diameter channels.

Thus, the channel structure is essentially 2D, with the most-open channels along one dimension. If charge transport depends strongly on the channel aperture, an anisotropic resistance would be expected. In view of the magnetic susceptibility data that is consistent with linear chain antiferromagnetic behavior and that correlates well with the channel area, it is reasonable to propose that the easy axis is close to the direction of largest aperture. According to this picture, the zigzag array of cavities, connected by 3.6-Å diameter channels, comprises both the dominant charge-transport and spin-exchange pathways. Partial alignment of the electrodes along the direction of the smaller, 2.3-Å diameter channels would result in a greater resistance. The longer, restrictive passages of diameter 0.8 Å that interconnect the 2D cavity−channel arrays account for the high impedance and the voltage-dependent behavior observed perpendicular to the crystal planes. Thus, the anisotropy of the impedance correlates well with the cavity−channel structure of $K^+(C222)e^-$, even though the absolute orientation of the electrodes with respect to the 3.6- and 2.3-Å channels remains uncertain.

Within the crystal plane, the low-frequency impedance decreases with an increase in temperature, although the resistance along the easy direction was so low that quantitative measurements were unreliable. Four-probe DC conductivity measurements along the hard in-plane axis as a function of temperature were carried out after the impedance measurements

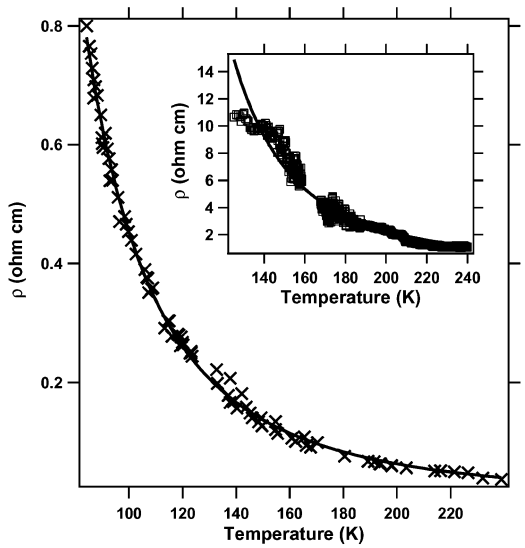

Figure 6. Resistivity of a powder sample of $K^+(C222)e^-$ as a function of temperature. The solid line is the best fit to the 2D hopping model. The inset shows the DC in-plane resistivity along the hard axis of a single crystal and the fit of a 2D hopping model.

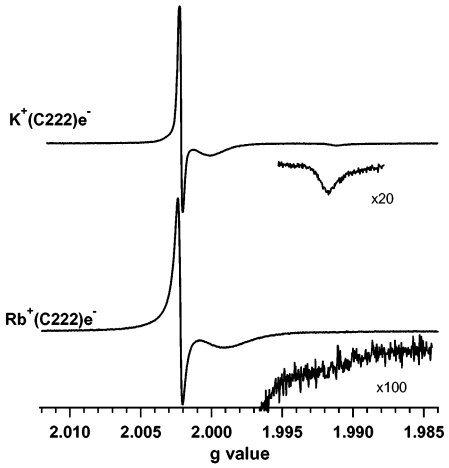

Figure 7. EPR spectrum of $K^+(C222)e^-$ and the β-phase powder of $Rb^+(C222)e^-$ at 10 K and low microwave power.

were completed. As with thin films and packed powders of this electride, the conductivity increased with increasing temperature. Over a similar temperature range, packed powders and thin films of the electride were found to have apparent sample-dependent activation energies. It was previously considered that the conductivity might be due to either activated (hopping) transport or the thermal population of a conduction band.[2,5] The preparation-dependent activation energy and the *increase* in conductivity during the early stages of decomposition of thin films suggested that defect percolation within the crystal is responsible for conduction.[5] The cavity−channel structure suggests that a 2D variable-range hopping model[24,25] would be appropriate. As shown in Figure 6, the conductivity of pressed pellets is well-described by a 2D hopping model, although the fit to a 3D model is also good. The inset to this Figure also shows that the DC conductivity along the hard direction is consistent with this model. The EPR measurements described below confirm the presence of at least two defects in the electride that may be involved in charge transport.

It is likely that a defect-free crystal of this electride would be a Mott insulator.[14] The energy cost of placing three electrons in the same cavity would be too great. However, a dumbbell cavity with only one electron instead of two would have a highly mobile hole that could readily move down the open chain. Defects in the chain, such as K^-, would block this motion and require activated hopping via the 2.3-Å channels to an adjacent chain. Hopping in the direction perpendicular to the crystal planes would be difficult because of the tortuous small channels in this direction. This model is in accord with both the defect-dependent conductivity and the preparation dependence of the apparent activation energy. It also explains why the resistivity of a relatively defect-free single crystal is higher than that of packed powders or polycrystalline films, both of which would be expected to have larger concentrations of defects.

EPR Spectra. The EPR spectra of crushed crystals of $K^+(C222)e^-$ and a polycrystalline sample of the β phase of $Rb^+(C222)e^-$ are compared in Figure 7. The similarity of the two spectra suggests that these signals have a common origin and adds further support to our hypothesis that the β phase of $Rb^+(C222)e^-$ has a similar structure to that of $K^+(C222)e^-$.[9] The EPR spectra of both electrides may be deconvoluted into two signals, a narrow Lorentzian ($g = 2.0022$) and an anisotropic signal with axial symmetry ($K^+(C222)e^-$: $g_{\text{parallel}} = 1.9912$, $g_{x,y} = 2.0016$; $Rb^+(C222)e^-$: $g_{\text{parallel}} \approx 1.99$, $g_{x,y} = 2.0014$). Electrides typically exhibit exchange-narrowed Lorentzian signals because exchange processes dominate along the cavity−channel directions. In addition, the resonances tend to be quite close to the free-electron g value because the trapped electrons are well-shielded from the alkali metal nuclei by the organic complexant molecules. The Lorentzian signals in Figure 7 have these same characteristics. However, the tensor components of the anisotropic signal are shifted away from the free-electron value, a behavior that has not been seen before with electrides. Furthermore, the line width of the $Rb^+(C222)e^-$ signal is larger than that of $K^+(C222)e^-$, and the g_{parallel} transitions in both spectra are weaker in intensity than would be predicted on the basis of the Zeeman part ($\beta_e\mathbf{H}\cdot\mathbf{g}\cdot\mathbf{S}$) of the spin Hamiltonian. The temperature dependence of the anisotropic signals suggests Curie-like behavior because the signal is most intense at 4 K but diminishes with increasing temperature until it is no longer observable above 60 and 100 K for $Rb^+(C222)e^-$ and $K^+(C222)e^-$, respectively. In contrast, the intensity of the signal at $g = 2.0022$ initially decreases in intensity as the temperature is raised and passes through a minimum around 100 K. Above 100 K, the intensity slowly increases, a behavior that mirrors the bulk magnetic susceptibility shown in Figure 2. Although the relative intensity of the Lorentzian and anisotropic signals differs from preparation to preparation, the temperature dependence for each is qualitatively the same.

Both EPR signals—the narrow Lorentzian and the axial g tensor—must be assigned to defect centers in the electride because the large value of the exchange constant, $-J \approx 300-450$ K, precludes significant intensity because of thermally excited states within a pure 1D chain at low temperatures (<100 K). The Lorentzian arises from electrons that are not subject to spin pairing, such as chain ends or cavity vacancies in which one electron occupies a two-electron site. These unpaired spins would be subject to exchange processes, however, that would account for the narrow line width. Single-electron cavities may be considered to contain holes rather than electrons because each cavity can accommodate two electrons. Hole percolation through the cavity−channel structure would then account for the high conductivity of $K^+(C222)e^-$ and $Rb^+(C222)e^-$ relative to the conductivity of electrides that have cavities that accommodate only one electron, such as $Cs^+(18\text{-crown-}6)_2e^-$.[13] Attempts to determine the sign of the carriers by measuring

the sign of the thermopower were unsuccessful in previous thin-film studies.[5]

The EPR signals with axial *g* anisotropy probably originate from a cavity that contains an electron plus K^- or Rb^-. In thin-film optical studies of K^+(C222)e^- and Rb^+(C222)e^-, films deposited at −60 °C had clear absorptions due to K^- and Rb^-, respectively.[5] The alkalide peaks disappeared as the films were annealed at −40 °C, and absorptions due to the electride simultaneously grew in. An electron that sits next to a heavy atom such as K^- or Rb^- would account for the substantial *g* shift and the axial *g* tensor. Within the confines of the roughly cylindrical cavity, an admixture of the electron's wave function with a vacant p orbital on the alkalide would introduce spin−orbit coupling that should be especially pronounced along the cavity or e^-−M^- axis. The expected outcome would be an axial or nearly axial *g* tensor. Because the spin−orbit interaction increases with increasing principal quantum number, the e^-−Rb^- pair should have the more perturbed *g* components, as observed. The difference in line width between the e^-−M^- defects in the electrides most likely arises from unresolved electron−nuclear hyperfine and/or quadrupolar interactions because the magnetogyric ratios and quadrupole moments of the rubidium isotopes are larger than those of potassium. In keeping with this interpretation, the weak *g*-parallel region is distinct in the K^+(C222)e^- spectrum but broadened almost beyond detection for Rb^+(C222)e^-. The line widths determined from simulations of the EPR spectra, especially for the perpendicular component (near the free-electron *g*-value), are 2.0 and 3.5 G for K^+(C222)e^- and Rb^+(C222)e^-, respectively. Peak-to-peak line widths of 0.43 and 0.6 G were used for the Lorentzian signals in the K^+(C222)e^- and Rb^+(C222)e^- simulations, respectively. Collectively, the *g* anisotropy, line widths, and temperature dependence of the EPR signals and the independent observations of K^- and Rb^- in unannealed thin films point to the presence of e^-−K^- and e^-−Rb^- pairs as defects in crystals of the potassium and rubidium electrides, respectively, grown from saturated solutions.

Saturation studies of these anisotropic defects in K^+(C222)e^- were carried out to determine if they would be suitable for ENDOR spectroscopy. However, instead of the anticipated saturation behavior that is characteristic of inhomogeneously broadened lines, the anisotropic EPR signal disappeared altogether when the microwave power was increased to 50 mW. This total disappearance was irreversible and happened within 20−40 s, the time required for a single field sweep. Electrides are strong microwave absorbers, and the exchange-narrowed singlets that are typically observed rarely saturate at high microwave power. Apparently, the sample was thermally annealed under the influence of the microwave radiation field in the EPR cavity, even at 4 K. Thermal annealing of M^- to e^- in electride thin films was also shown to be irreversible.[5] Accompanying the loss of the broad EPR signal was a concomitant gain in intensity of the $g = 2.0022$ signal. In order for the annealing process to be irreversible, the alkalide would probably yield two electrons plus the cation, M^+. The latter would then be trapped by a vacant complexant molecule.

An interesting question is how alkalide defects in K^+(C222)e^- crystals would affect charge transport. In thin-film studies that combined optical spectroscopy and four-probe DC conductivity measurements,[5] the conductivity of a given film was essentially the same before and after annealing even though the electride peak clearly grew in intensity and the K^- peak disappeared. The major contributor to activated transport may simply be the number of hole defects created during crystal growth, a quantity that varies from one synthesis to another.

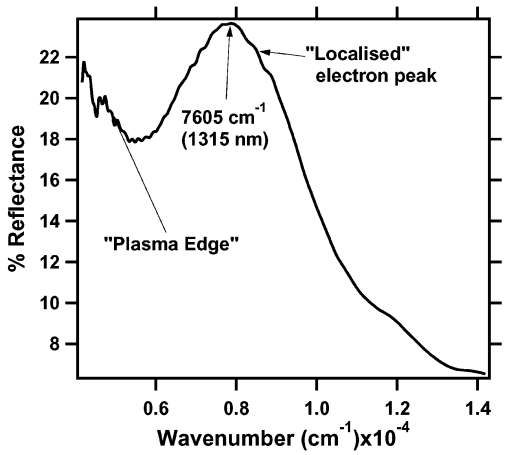

Figure 8. Single-crystal reflectance spectrum of K^+(C222)e^-.

Optical Spectrum. The single-crystal reflectance spectrum taken at −60 °C with unpolarized light is shown in Figure 8. The spectrum consists of a typical localized electron peak at 7605 cm^{-1} (1315 nm) due to trapped electrons and a rise in the percent reflectance toward the mid-IR (<6000 cm^{-1}). This portion of the spectrum was previously identified as a plasma edge typically observed in the reflectance spectra of conductors. The spectrum in Figure 8 is nearly identical to those obtained from thin films of both K^+(C222)e^- and Rb^+(C222)e^- after annealing a film prepared at −60 °C or when the electride film is deposited on the substrate at −40 °C.[5] The spectrum is reminiscent of the reflectance spectra of metal ammonia solutions just above the nonmetal-to-metal transition.[26] The reflectance measurement confirms that the NIR peak and plasma edge are intrinsic properties of the K^+(C222) electride.

Discussion

Thin films and packed powders are polycrystalline in nature and may contain more defects that contribute to the conductivity, especially at grain boundaries. However, the single-crystal impedance measurements confirm that activated transport is a property intrinsic to crystals and not an artifact of polycrystalline composition. Two different mechanisms of charge transport may operate within and between the planes formed by the cavities and channels. On the basis of EPR measurements, one type of defect corresponds to cavity vacancies or holes in which only one electron occupies a two-electron site. Hole percolation may be the dominant conduction mechanism through the open-cavity−channel arrays. Whereas the 2D arrays of cavities and channels have conducting or semiconducting properties, the interlayer separation is apparently insulating. The distance between cavity−channel layers is less than 10 Å, and so tunneling between the 2D cavity−channel layers may occur and result in the high impedance and voltage-dependent behavior perpendicular to the crystal plane.

Acknowledgment. This work was supported in part by the U.S. National Science Foundation under grant no. DMR 9988881.

References and Notes

(1) Huang, R. H.; Faber, M. K.; Moeggenborg, K. J.; Ward, D. L.; Dye, J. L. *Nature (London)* **1988**, *331*, 599−601.

(2) Moeggenborg, K. J.; Papaioannou, J.; Dye, J. L. *Chem. Mater.* **1991**, *3*, 514−520.

(3) Wagner, M. J. Ph.D. Dissertation, Michigan State University, East Lansing, MI, 1994.

(4) Dye, J. L.; Wagner, M. J.; Overney, G.; Huang, R. H.; Nagy, T. F.; Tomanek, D. *J. Am. Chem. Soc.* **1996**, *118*, 7329−7336.

(5) Hendrickson, J. E.; Pratt, W. P., Jr.; Phillips, R. C.; Dye, J. L. *J. Phys. Chem. B* **1998**, *102*, 3917−3926.

(6) Bonner, J. C.; Fisher, M. E. *Phys. Rev. A: At., Mol., Opt. Phys.* **1964**, *135*, 640−658.

(7) Bonner, J. C.; Blote, H. W. J.; Bray, J. W.; Jacobs, I. S. *J. Appl. Phys.* **1979**, *50*, 1810−1812.

(8) Dye, J. L. *Inorg. Chem.* **1997**, *36*, 3816−3826.

(9) Xie, Q.; Huang, R. H.; Ichimura, A. S.; Phillips, R. C.; Pratt, W. P., Jr.; Dye, J. L. *J. Am. Chem. Soc.* **2000**, *122*, 6971−6978.

(10) Wagner, M. J.; Dye, J. L. In *Molecular Recognition: Receptors for Cationic Guests*, 1st ed.; Gokel, G. W., Ed.; Pergamon Press: Oxford, U.K., 1996; Vol 1, pp 477−510.

(11) Singh, D. J.; Krakauer, H.; Haas, C.; Pickett, W. E. *Nature (London)* **1993**, *365*, 39−42.

(12) Dye, J. L. *Nature (London)* **1993**, *365*, 10−11.

(13) Wagner, M. J.; Ichimura, A. S.; Huang, R. H.; Phillips, R. C.; Dye, J. L. *J. Phys. Chem. B* **2000**, *104*, 1078−1087.

(14) Mott, N. F. *Can. J. Phys.* **1956**, *34*, 1356.

(15) Wagner, M. J.; Huang, R. H.; Eglin, J. L.; Dye, J. L. *Nature (London)* **1994**, *368*, 726−729.

(16) Wagner, M. J.; Dye, J. L. *J. Solid State Chem.* **1995**, *117*, 309−317.

(17) Huang, R. H.; Ward, D. L.; Dye, J. L. *J. Am. Chem. Soc.* **1989**, *111*, 5707−5708.

(18) Dye, J. L. *Prog. Inorg. Chem.* **1984**, *32*, 327−441.

(19) Dye, J. L. *J. Phys. Chem.* **1984**, *88*, 3842−3846.

(20) Ward, D. L.; Huang, R. H.; Dye, J. L. *Acta Crystallogr., Sect. C* **1988**, *44*, 1374−1376.

(21) Kuo, C.-T. Ph.D. Dissertation, Michigan State University, East Lansing, MI, 1994.

(22) Hall, J. W.; Marsh, W. E.; Weller, R. R.; Hatfield, W. E. *Inorg. Chem.* **1981**, *20*, 1033−1037.

(23) Huang, R. H.; Wagner, M. J.; Gilbert, D. J.; Reidy-Cedergren, K. A.; Ward, D. L.; Faber, M. K.; Dye, J. L. *J. Am. Chem. Soc.* **1997**, *119*, 3765−3772.

(24) Mott, N. F. *Philos. Mag.* **1969**, *19*, 835.

(25) Brenig, W.; Dohler, G. H.; Heyszenau, H. *Philos. Mag.* **1973**, *27*, 1093.

(26) Beckman, T. A.; Pitzer, K. S. *J. Phys. Chem.* **1961**, *65*, 1527−1532.